

Halogen Bonds between 2,2,6,6-Tetramethylpiperidine-*N*-oxyl Radical and C_xH_yF_zI Species: DFT Calculations of Physicochemical Properties and Comparison with Hydrogen Bonded Adducts

Paola Cimino,^{*,†,‡} Michele Pavone,[†] and Vincenzo Barone[‡]

Dipartimento di Chimica, Università di Napoli Federico II, Complesso Universitario Monte S. Angelo, via Cintia, I-80126, Napoli, Italy, and Dipartimento di Scienze Farmaceutiche, Università di Salerno, via Ponte don Melillo, 84084, Fisciano (Sa), Italy

Received: May 10, 2007; In Final Form: June 28, 2007

Structural, thermodynamic, and magnetic properties of adducts between the 2,2,6,6-tetramethylpiperidine-*N*-oxyl radical and representative hydrogen and halogen bond donors in solution have been investigated by an integrated computational tool including hybrid density functionals and discrete-continuum solvent models. From a quantitative point of view, the computed values show a fair agreement with experiment when environmental effects are taken into the proper account. From a more general point of view, our analysis points out a number of analogies, but also some difference, between hydrogen and halogen bond, which have been interpreted in terms of the various effects tuning thermodynamic and spectroscopic parameters.

1. Introduction

Interest in nitroxide radicals stems from their prominent role as spin labels in biology, biochemistry, and biophysics to monitor the structure and the motion of biological molecules and membranes, as well as nanostructures.^{1,2} Indeed, labeling of specific sites by nitroxide probes allows effective structural and dynamic analyses by means of EPR and ENDOR spectroscopies, thanks to the sensitivity of some magnetic parameters (e.g., gyromagnetic and nuclear hyperfine tensors) to interactions with the surrounding molecules and to the polarity of the local environment.³

In this connection, the ability of the NO moiety to interact with hydrogen-bond donors is particularly significant, since it leads to a fine-tuning of the physicochemical properties of nitroxides under controlled conditions.^{4,5} The hydrogen atom is the most common electron-acceptor site, and hydrogen bonding (HB) is the most frequently occurring noncovalent interaction in chemical and biological processes. Halogen atoms equally work as acceptors and the interaction (halogen bond, XB), which they give rise to, seems to be characterized by several properties similar to those of the hydrogen bond.⁶ Advanced studies have extensively proven the crucial role played by interatomic interactions involving halogen atoms in macromolecular structures (proteins, nucleic acids, polymeric materials), e.g. in stabilization of bioactive forms,⁷ in molecular recognition,⁸ and in crystal engineering.⁹

The interaction of the quite stable TEMPO radical (2,2,6,6-tetramethylpiperidine-*N*-oxyl) with several iodine-substituted fluoroalkanes and fluorobenzenes has been recently investigated¹⁰ for the first time by EPR spectroscopy: halogen bonding to different XB donors can show a strength comparable to hydrogen bonding (in terms of equilibrium constants and other thermodynamic parameters). Such an approach complements other analytical methods used till now to detect XB formation,

to define its nature, to establish its strength and structure, and to reveal the similarities between XB and HB. Therefore, in order to gain further insights into the features of this intermolecular interaction, particularly in terms of electron spin transfer from radical (electron donor) to halogenated molecules (electron acceptors), a reliable quantum-mechanical (QM) method could be a valuable tool toward an integrated experimental and computational approach.

High-field EPR spectroscopy provides quite rich information consisting essentially of the nitrogen hyperfine (A_N) and gyromagnetic (g) tensors. However, interpretation of these experiments in structural terms strongly benefits from quantum chemical calculations able to dissect the overall observables in terms of the interplay of several subtle effects. The QM computation of nuclear hyperfine tensors has a long history,^{11–14} which has finally led to the development of cost-effective and reliable approaches,¹¹ whereas quantitative calculations of g tensor for large molecules, by the machinery of nonempirical quantum chemistry, have become possible only recently.¹⁵ The calculation and interpretation of g tensors for HB and XB complexes with large spin probes are very important in so many fields that the development and validation of suitable theoretical approaches for the determination of magnetic properties is becoming a crucial step.

Methods rooted in the density functional theory (DFT) coupled to purposely tailored basis sets are generally able to reproduce with good accuracy the structures and properties of organic free radicals in the gas phase.¹¹ Inclusion of bulk solvent effects by implicit models like the so-called polarizable continuum model, PCM,^{16,17} leads to good results for non-hydrogen-bonding solvents, whereas inclusion of some explicit solvent molecules (together with the continuum) is mandatory in the case of hydrogen-bonding solvents.^{11,18,19} This latter approach is particularly effective in view of the reduced number of solvent molecules to be considered^{19,20} and of the effectiveness of the latest implementations of PCM.²¹ In this way, solvent shifts on g ²² and hyperfine tensors (A_X)^{19,20} are usually reproduced with good accuracy.

* Corresponding author. E-mail: cimino@unisa.it

† University of Napoli "Federico II".

‡ Permanent address: University of Salerno.

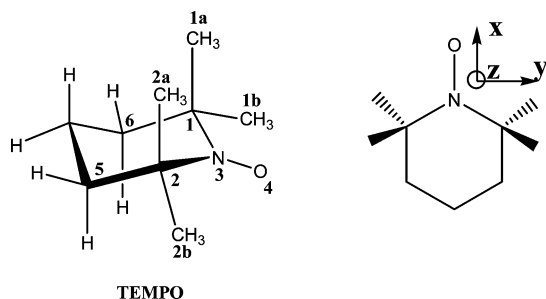


Figure 1. Structure of TEMPO (2,2,6,6-tetramethylpiperidine-*N*-oxyl) radical.

We have recently validated a general computational approach to the analysis of spin-probing and spin-labeling experiments, by providing an accurate description of thermodynamic and spectroscopic properties of adducts of TEMPO with HB donors.²⁰ Here, we extend the study to intermolecular interactions between TEMPO and several hydrogen- and halogen-bond donors, in order to evaluate the role of different electron acceptors on the adduct geometry and on the strength of the interaction, by means of an accurate estimation of thermodynamic and spectroscopic properties. Computed and experimental magnetic tensors for different HB and XB species are quite similar. Together with well-known trends, the correlation between the isotropic part of the **g** tensors (and its g_{xx} component directed along the NO bond) and the intermolecular CNO...I/OH dihedral angle will be discussed. Our general aim is to provide a quantitative interpretation of nitroxide sensitiveness to the polarity of the local environment and, especially, to interactions with surrounding molecules, i.e., hydrogen/halogen bonds. The characteristics of these systems are investigated by the so-called natural bond orbitals (NBO) approach. We believe that these results can be useful for a sound interpretation of experimental EPR data, allowing the relation of the observed parameter shifts to specific local and environmental effects.

2. Methods

All the calculations were carried out by the Gaussian 03 package²³ using the PBE0 hybrid density functional²⁴ with Pople's basis sets ranging from 6-31G(d) to 6-311++G(2d,-2p),²⁵ together with our EPR-II, EPR-III,^{12,26} and N06²⁷ basis sets. The last basis set was obtained by adding to a double- ζ description of valence orbitals single sets of optimized core-valence *s* (on all atoms except H), diffuse *s* (on H), diffuse *p* (on all atoms except H), polarization (on all atoms), and diffuse *d* (on N, O, F, I atoms) functions. The inner electrons of C, N, O, F atoms were described by the 6G basis set, whereas those of the I atom were replaced by the Stuttgart effective potentials (SDD).²⁵ The PBE0/N06 model leads at the same time to improved geometries, EPR parameters, and strongly reduced basis set superposition error (BSSE). Bulk solvent effects have been taken into account by the PCM,^{17,21} in which the solvent is represented by an infinite dielectric medium characterized by the relative dielectric constant of the bulk, and the UAHF radii²⁸ are used for building the effective cavity occupied by the solute in the solvent.

Geometry optimizations and evaluations of harmonic frequencies have been performed at the PBE0/6-31G(d) level in the gas-phase and at the PCM-PBE0/6-31G(d) level in solution. The binding energy (ΔE) of each complex is calculated as the difference between the total energy of the complex and the sum of the monomers' total energies correcting the BSSE by the counterpoise method.²⁹ General trends have been further analyzed by the NBO approach.³⁰

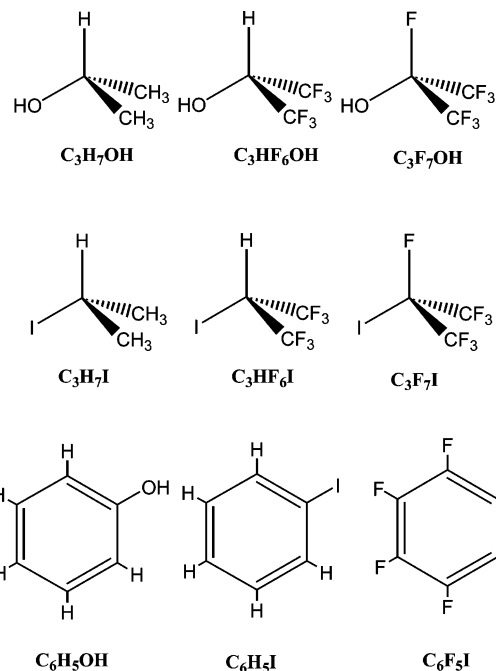


Figure 2. Structures of the studied protonated and halogenated molecules.

Nuclear hyperfine and gyromagnetic tensors have been computed at PBE0/6-31G(d) geometries by the N06 and EPR-II basis sets following well-defined procedures described in recent literature.^{12,22}

The hyperfine coupling tensor (\mathbf{A}_X), which describes the interaction between the electronic spin density and the nuclear magnetic momentum of nucleus X, can be split into three terms, $\mathbf{A}_X = a_X \mathbf{I}_3 + \mathbf{T}_X + \mathbf{\Lambda}_X$, where \mathbf{I}_3 is the 3×3 unit matrix. The first term (a_X), usually referred to as the Fermi-contact interaction, is an isotropic contribution, also known as the hyperfine coupling constant (hcc), and is related to the spin density at the corresponding nucleus X. The second contribution (\mathbf{T}_X) is anisotropic and can be derived from the classical expression of interacting dipoles. The last term, $\mathbf{\Lambda}_X$, is due to second-order spin-orbit coupling and can be determined by methods similar to those described in the following for the gyromagnetic tensor. In the present case, because of the strong localization of spin density on second-row atoms and of their small spin-orbit coupling constants, its contribution can be safely neglected and will not be discussed in the following. Of course, upon complete averaging by rotational motions, only the isotropic part survives. Because both a_X and \mathbf{T}_X are ruled by one-electron operators, their evaluation is, in principle, quite straightforward. However, hyperfine coupling constants have been among the most challenging quantities for conventional QM approaches for two main reasons.¹¹ On one hand, conventional Gaussian basis sets are ill-adapted to describe nuclear cusps and, on the other hand, the overall result derives from the difference between large quantities of opposite sign. However, the past few years have shown that coupling of some hybrid functionals (here PBE0)²⁴ to purposely tailored basis sets (here EPR-II)¹² performs a remarkable job both for isotropic and dipolar terms. In the case of nitroxides, the key terms are those of the nitrogen atom (a_N and \mathbf{T}_N) and are usually given in gauss (1 G = 0.1 mT).

The gyromagnetic tensor can be written as $\mathbf{g} = g_e \mathbf{I}_3 + \Delta \mathbf{g}_{RM} + \Delta \mathbf{g}_G + \Delta \mathbf{g}_{ZSOC}$, where g_e is the free-electron value ($g_e = 2.0023193$). Computation of the relativistic mass (RM) and gauge (G) corrections is quite straightforward, because they are first-order contributions.^{15a,b} The last term arises from the

TABLE 1: Computed Geometrical Parameters (distances in Å and angles in degrees) for TEMPO with Different Basis Sets and the PBE0 Functional

basis functions	atoms	N3–O4	C1–N3/C2–N3	C1–C1a/C2–C2a	C1–C1b/C2–C2b	C1–N3–C2	C1–N3–O4–C2
6-31G(d)	N, O, C, H	1.274	1.489/1.489	1.528	1.534	124.4	157.9
6-31+G(d,p)	N, O, C, H	1.274	1.491/1.491	1.529	1.536	124.3	158.2
6-311G(d,p)	N, O, C, H	1.268	1.491/1.491	1.527	1.533	124.3	157.9
6-311+G(d,p)	N, O, C, H	1.268	1.491/1.491	1.527	1.533	124.2	158.3
6-311++G(2d,2p)	N, O, C, H	1.269	1.490/1.490	1.529	1.536	124.3	158.4
N06	N, O, C, H	1.268	1.490/1.490	1.526	1.533	124.1	158.1
N06	N, O	1.268	1.491/1.491	1.529	1.535	124.1	158.2
6-31G(d)	C, H						

TABLE 2: Calculated Intermolecular N···I Distance (Å) for the Complex CF₃I···N(CH₃)₃

	N···I distance
B3LYP/3-21G(d)	2.709 ^a
B3LYP/Ahlrichs on H,C,N,F atoms	2.714 ^a
B3LYP/LanLDZdp ECP on I atom	
B3LYP/Ahlrichs on H,C,N,F atoms	2.720 ^a
B3LYP/Stuttgart RLC ECP on I atom	
B3LYP/6-31G(d) on H,C,N,F atoms	2.931 ^a
B3LYP/6-311G(d) on I atom	
B3LYP/N06	2.864
PBE0/N06	2.782
exp ^b	2.84 ± 0.03

^a Reference 31a. ^b Reference 31b.

coupling of the orbital Zeeman (OZ) and the spin-orbit coupling (SOC) operator. The OZ contribution is computed using the gauge-including atomic orbital (GIAO) approach,^{15c} whereas the two-electron SOC operator is approximated by a one-electron operator involving adjusted effective nuclear charges.^{15a,d} Upon complete averaging by rotational motions, only the isotropic parts of \mathbf{A}_N and \mathbf{g} tensors survive, which are given by $a_N = \frac{1}{3}\text{Tr}(\mathbf{A}_N)$ and $g_{\text{iso}} = \frac{1}{3}\text{Tr}(\mathbf{g})$. The isotropic part of the hyperfine tensor is usually referred to as hyperfine splitting or the hyperfine coupling constant and will be given in the following in gauss. The isotropic part of the gyromagnetic tensor is given in the following in terms of shift from the free electron value, $\Delta g_{\text{iso}} = g_{\text{iso}} - g_e$, and is expressed in parts per million (ppm).

3. Results

In a previous work,²⁰ we validated the integrated DFT/PCM approach for the computation of thermodynamic and spectroscopic properties of the complex between TEMPO (Figure 1) and alcohols (phenol, benzylic alcohol). Here, we further validate the proposed approach through the analysis of different basis sets and density functionals and by comparing two different classes of electron acceptors, namely alcohols and halogenated molecules (Figure 2): aliphatic and aromatic alcohols form conventional H-bonds with different strengths, whereas the analogous halogenated species allow us to describe the basic features of the “halogen bond”.

First, we tested a variety of basis sets for the geometrical parameters of the bare TEMPO radical. Inspection of Table 1 reveals that the recently developed N06 basis set predicts geometrical parameters in close agreement with the benchmark data, corresponding to the 6-311++G(2d,2p) basis set, at a significantly reduced computational cost. Further calculations have been carried out to evaluate the performance of the new basis set in the description of the intermolecular parameters of donor-acceptor pairs (Table 2): concerning the intermolecular distance in the complex between N(CH₃)₃ and CF₃I, our method reproduces the experimental data (2.864 vs 2.84 ± 3 Å) better than previous computations employing similar or larger basis

TABLE 3: Geometric Parameters for the TEMPO–C₆F₅I Complex

	NO···I distance (Å)	NO···I angle (deg)	CNO···I angle (deg)
B3LYP/N06	2.956	145.2	94.0
PBE0/N06	2.883	140.8	95.3
exp (ref 32)	2.827(9)	145.0	80.1

TABLE 4: Uncorrected (ΔE) and BSSE-Corrected (ΔE^{BSSE}) Interaction Energies (kcal/mol) for TEMPO–Phenol Complex Optimized with PBE0 Functional and Different Combinations of Basis Sets in the Gas Phase

basis set	ΔE	ΔE^{BSSE}
6-31G(d) on all atoms	−10.92	−7.94
N06 on all atoms	−9.47	−8.35
N06 on N, O and acid H atoms	−9.45	−8.18
6-31G(d) on all others atoms		

TABLE 5: Nitrogen Isotropic Hyperfine Splitting (a_N in G) and Isotropic g Tensor Shifts (Δg_{iso} in ppm) Values for TEMPO Computed with PBE0 and B3LYP Functionals and Different Combinations of Basis Sets in the Gas phase

	a_N	Δg_{iso}
PBE0/EPR-II//PBE0/6-31G*	12.78	2.00624
PBE0/EPR-III//PBE0/N06	12.74	2.00632
(B3LYP/EPR-III//B3LYP/N06)	(12.49)	(2.00644)
PBE0/EPR-II//PBE0/N06	12.67	2.00619
(B3LYP/EPR-II//B3LYP/N06)	(12.43)	(2.00626)
PBE0/N06//PBE0/6-31G*	14.92	2.00610
PBE0/N06 (N, O, C1, C1a, C1b, C2, C2a, C2b, C5, C6) + 6-31G(d) (other atoms)//PBE0/6-31G(d)	14.93	2.00606
PBE0/N06 (N, O, C1, C2) + 6-31G(d) (other atoms)//PBE0/6-31G(d)	14.96	2.00606
PBE0/N06 (N, O) + 6-31G* (other atoms)//PBE0/6-31G*	14.96	2.00605
PCM/PBE0/N06//PBE0/6-31G* (cyclohexane)	15.23	2.00601
experimental (cyclohexane)	15.28	

sets.³¹ A comparison between calculated and experimental³¹ structures for the complex TEMPO–C₆F₅I (Table 3) shows that the agreement, though not perfect, should be largely sufficient for a systematic study aimed to analyze general trends.

A comparison of the formation energies of the TEMPO–phenol complex computed by different basis sets (Table 4) shows that use of the N06 basis set for nitrogen, oxygen, and halogen atoms and of the cheaper 6-31G(d) basis set for C and H atoms allows a non-negligible saving of computer time without any appreciable degradation of binding energies or increase of the BSSE. Next, the nitrogen hyperfine coupling constant (a_N) and \mathbf{g} tensors of the TEMPO radical have been evaluated by several combinations of basis sets. Our results, listed in Table 5, show that reliable magnetic properties can be obtained only by treating at high level at least all the atoms giving a non-negligible contribution to the formally singly occupied molecular orbital (SOMO, see Figure 4), namely, the

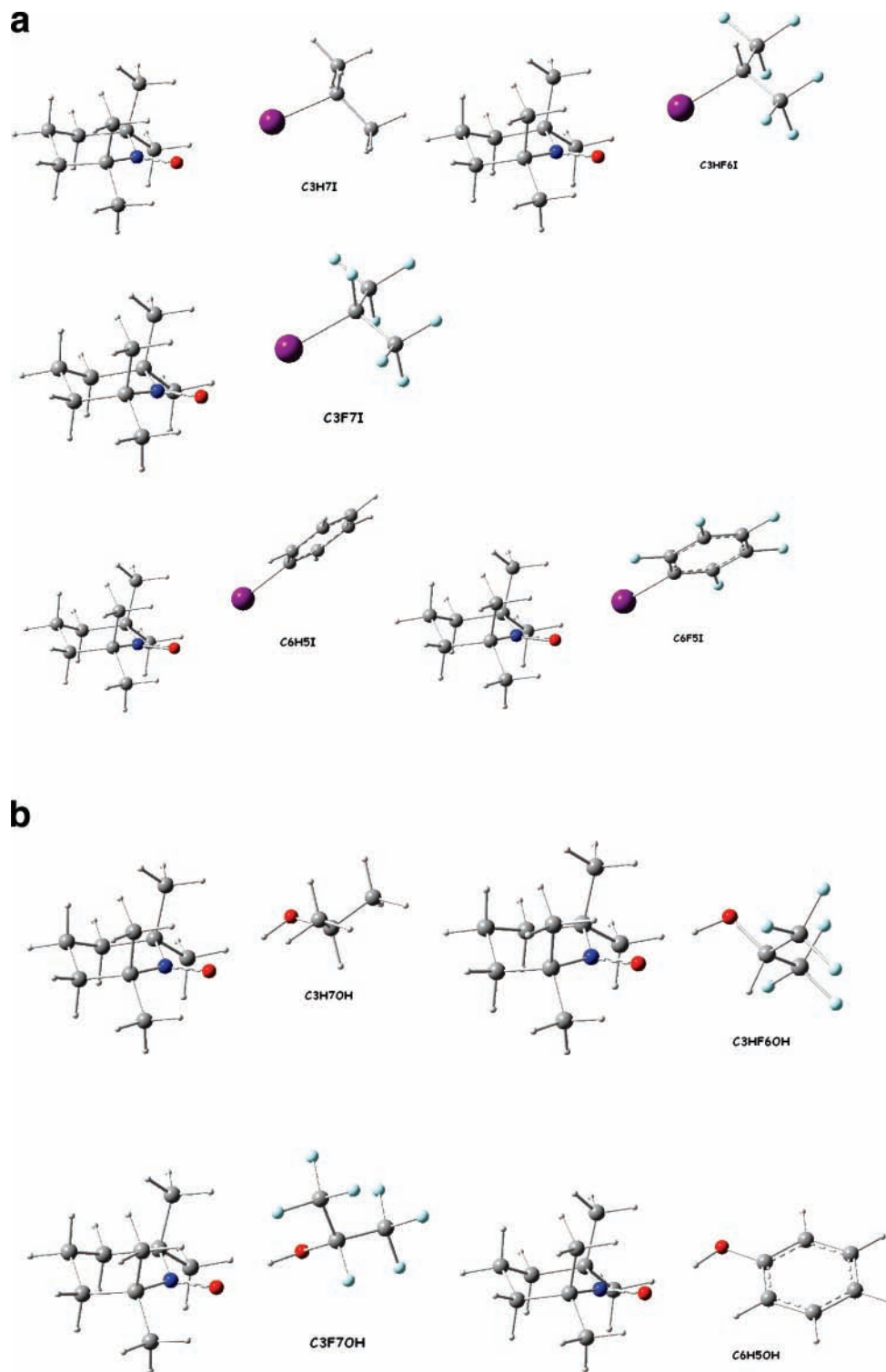


Figure 3. (a) Optimized structures of the TEMPO–iodo derivative complexes. (b) Optimized structures of the TEMPO–alcohol complexes.

NO moiety, the two nearest carbon atoms (1 and 2), and the methyl carbons (1a,1b, 2a, 2b), while using the 6-31G(d) basis set for the other atoms. Thus, all the following computations will be performed using this composite basis set.

3.1. Geometric Structures and Interaction Energies. As mentioned in the Introduction, we focused our attention on the formation of complexes of TEMPO with iodoalkanes, perfluoroiodoalkanes, iodobenzenes, perfluoroiodobenzenes, and the corresponding alcohols (sketched in Figure 2). In particular, we choose perfluoroiodoalkanes and perfluoroiodobenzenes because it was experimentally demonstrated¹⁰ that they behave as strong electron acceptors in XB interactions. DFT calculations led to

the optimized structures shown in Figure 3, the most important geometrical parameters of which are collected in Table 6 together with the computed binding energies. Experimental data^{10,20} indicate the following interaction energy trends: derivatives with F > derivatives without F; perfluoroalkyl > perfluoroaromatic and alcohol complexes > iodo complexes. The calculated interaction energies show the same trend, although from a quantitative point of view the agreement is not perfect. This is well-evidenced, for instance, by comparison between the computed binding energies (−9.97, −8.38 kcal/mol) and the experimental ΔH 's (−5.46, −4.69 kcal/mol)¹⁰ of C₃HF₆OH and phenol. Since the quality of the density functional

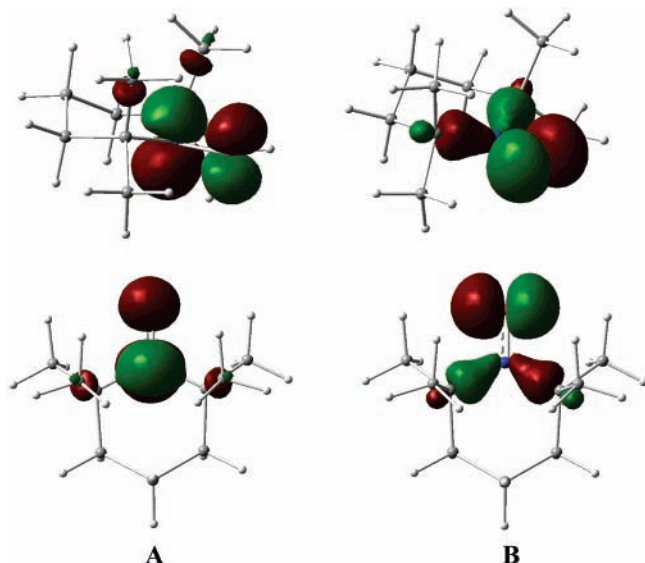


Figure 4. Sketch of SOMO (A) and SOMO-1 (B) of TEMPO in two different orientations.

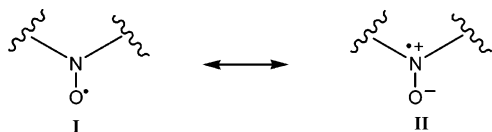


Figure 5. Principal resonance structures of a nitroxide radical.

and basis set have been carefully checked, the remaining disagreement with experiments is related, in our opinion, to the neglect of dynamical effects leading to thermal averaging between different structures. While these effects can be taken into account by suitable molecular dynamics simulations,³³ this is beyond the purposes of the present study.

We will not discuss structural parameters in detail since, as previously reported for complexes with alcohols, they are in general agreement with experimental results.^{9,10} The binding energies (Table 6) lie in the ranges 1.3–4.9 kcal/mol and 7.5–10.3 kcal/mol, respectively, for the complexes with iodine derivatives and alcohols, and there is an increment (in absolute value) of about 0.5 kcal/mol for each F atom. The increase of binding energies when going from iodo derivatives to alcohols is paralleled by a contraction in the NO \cdots I/OH intermolecular distance. The strength of the NO \cdots H bond is larger in the complexes formed by TEMPO with perfluorinated alcohols than in those with analogous molecules without fluorine atoms (for example, 1.870 Å for C₃H₇OH vs 1.663 Å for C₃F₇OH). This reflects the closeness to the –OH moiety of strong electron-withdrawing functional groups, like fluorine atoms. It must also be noted that a slightly larger NO lengthening is connected to formation of hydrogen bonds, with respect to halogen bonds. Concerning the bond strengths of perfluorinated iodine compounds, our results indicate that TEMPO–XB complexes are less stable than the corresponding TEMPO–HB ones and that bulk solvent effects on the hydrogen-bond strengths are not negligible.

The NBO analysis³⁰ allows analysis of how the influence of fluorine atoms on the properties of the I and OH groups affects their acceptor ability. The localized orbitals issuing from the NBO analysis are the σ_{NO} and π_{NO} bonding orbitals, together with two sp^2 oxygen lone pairs (LP1 and LP2) and the π_{NO}^* singly occupied molecular orbital (SOMO). In the isolated TEMPO radical, the contribution of the N atom to the bonding π_{NO} orbital is slightly larger than that of the O atom (52.1%

versus 47.9% for the oxygen). The situation is reversed when the radical is involved in the intermolecular interaction with alcohols or iodine derivatives (for example, 47.5% for N versus 52.5% for O in the complex between TEMPO and C₃F₇I), and this is accompanied by a charge transfer to the electron acceptor. A summary of the NBO description of the –NO \cdots I/OH interaction energies is given in Table 7. We recall that the sum of the delocalization contributions issuing from the second order of perturbation theory, $E^{(2)}$, provides a reliable estimate of the total charge-transfer energy.² The $E^{(2)}$ issuing from the interaction of TEMPO π_{NO}^* orbital and oxygen lone pairs (LP_{tot}) with the electron acceptor group, LP_{tot} \rightarrow (C–I/OH)^{*}, is significantly more important in fluorine complexes than in hydrogen ones, indicating that, as suggested by chemical intuition, the electron-acceptor ability of I/OH increases with the number of F atoms. Moreover, intermolecular charge transfer is more important for the TEMPO–alcohol complexes than for the TEMPO–iodo derivatives (for example, 8.4 kcal/mol for C₃F₇I vs 37.1 kcal/mol for C₃F₇OH). Figure 6 displays the total $E^{(2)}$ contribution versus the intermolecular distance, for the complexes between TEMPO and alkane derivatives. These results are consistent with the fact that a shortening of the NO \cdots I/OH contact corresponds to a larger intermolecular energy. The behavior of the quantities listed in Table 7, as a function of the NO \cdots I/OH distance, shows how the different interactions operate and how they affect magnetic properties (see the next section).

3.2. Spectroscopic Parameters. First, let us recall that the “magnetic orbitals” (see below for a more detailed definition) of nonconjugated nitroxides are strongly localized onto the NO moiety (Figure 4), so that the principal axes of both hyperfine and **g** tensors are well-aligned with the NO bond (by convention *x*-axis) and with the average direction of π orbitals (*z* axis). Since this conventional reference frame nearly coincides with the principal inertia frame, off-diagonal tensor elements can be safely neglected in the interpretation of EPR and ENDOR spectra. Furthermore, the largest component of the ¹⁴N hyperfine tensor (**A**_{N,*zz*}) conveys all the information about dipolar interactions. Since both direct and spin-polarization contributions to the ¹⁴N isotropic hyperfine splitting (*a*_N) are roughly proportional to the spin population in the π_{NO}^* SOMO (Figure 4), *a*_N and **A**_{N,*zz*} show closely parallel trends. As a consequence, the discussion will be concentrated on *a*_N (which shows stronger solvent shifts and more direct connection with experimental results). In the same vein, the behavior of the **g** tensor is dominated by its largest component *g*_{*xx*} (vide infra), so that Δg_{iso} and *g*_{*xx*} show parallel trends.

Table 8 lists the experimental and computed *a*_N values for all the complexes in the gas phase (EPR-II and N06 basis sets) and in solution (N06 basis set). Till now, accurate estimates were obtained only using very demanding theory levels, e.g., quadratic configuration interaction including single and double excitations (QCISD)^{34,35} with purposely tailored basis sets,^{26,36} possibly integrated into an ONIOM-like approach.¹¹ It is thus particularly significant that PBE0/N06 computations are in close agreement with experiment without any further correction, more so as also the trends of the values calculated in solution fit quite well their experimental counterparts. Note that, as discussed in detail in previous papers, and contrary to five-membered rings, the quite rigid backbone of piperidine derivatives leads to negligible vibrational averaging effects on isotropic hyperfine coupling constants.^{3,11}

The nitrogen hyperfine coupling constant (Table 8) increases with the dielectric constant of the solvent and also with the number of F atoms in the hydrogen or halogen bond partner.

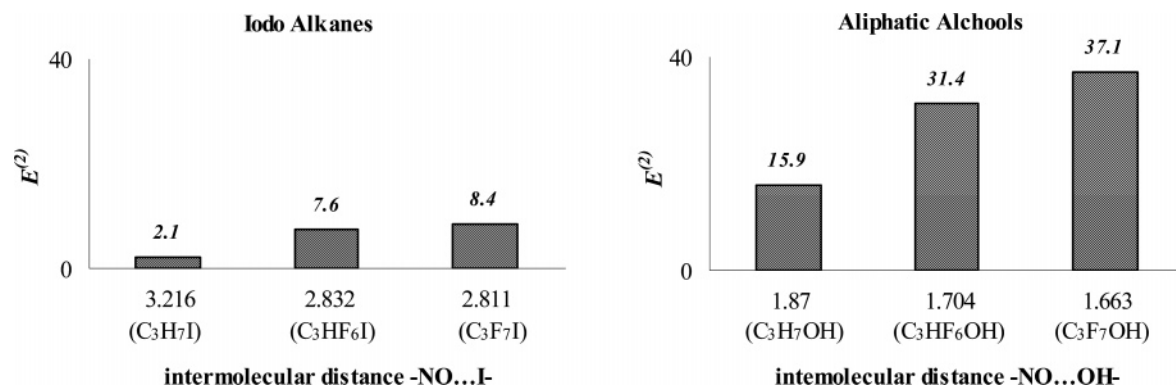


Figure 6. Stabilization energy ($E^{(2)}$) in kcal/mol vs the intermolecular distance (in Å) in the complexes TEMPO–iodoalkanes and TEMPO–alcohols.

TABLE 6: Interaction Energies and Geometrical Parameters for All Complexes Calculated with PBE0 Functional with 6-31G(d) for C, H Atoms and N06 for N, O, and Halogen Atoms in the Gas Phase and in Solution

	C ₃ H ₇ I	C ₃ HF ₆ I	C ₃ F ₇ I	C ₆ H ₅ I	C ₆ F ₅ I	C ₆ H ₅ OH	C ₃ H ₇ OH	C ₃ HF ₆ OH	C ₃ F ₇ OH
ΔE (kcal/mol)									
gas phase	-1.32	-4.87	-5.36	-2.45	-4.78	-8.38	-7.54	-9.97	-10.30
CHCl ₃	-0.14	-3.24	-3.92	-1.30	-3.16	-3.89	-3.54	-5.29	-6.54
ε = 4.9									
C ₂ H ₄ Cl ₂	0.07	-2.83	-3.53	-1.08	-2.76	-2.67	-2.54	-3.83	-5.49
ε = 10.36									
ethanol	0.22	-2.48	-3.19	-0.88	-2.42	-1.88	-1.86	-3.01	-4.67
ε = 24.55									
Distance (Å)									
NO	1.269	1.269	1.269	1.268	1.268	1.271	1.270	1.271	1.271
NO→I	3.216	2.832	2.811	3.036	2.840	1.790	1.870	1.704	1.663
Angle (deg)									
NO···I	144.1	142.9	142.9	137.8	139.9	132.3	131.4	132.0	135.6
CNO···C	21.0	17.9	17.6	19.7	17.7	19.0	19.4	18.6	18.0
CNO···I	28.3	51.6	51.6	79.2	95.4	16.4	19.5	16.3	12.1

TABLE 7: NBO Stabilization Energies in kcal/mol (second-order perturbation energy, $E^{(2)}$) for All Complexes Computed at PBE0/NO6 Level on Geometries Optimized at the PBE0/6-31G(d) Level

$E^{(2)}_{LP-(C-I/OH)^*}$	C ₃ H ₇ I	C ₃ HF ₆ I	C ₃ F ₇ I	C ₆ H ₅ I	C ₆ F ₅ I	C ₆ H ₅ OH	C ₃ HF ₆ OH	C ₃ F ₇ OH	C ₆ H ₅ OH
LP1 ↑	0.49	0.93	1.10	0.60	0.90	0.27	0.17	0.15	0.76
LP1 ↓	0.69	2.05	2.17	1.09	2.15	3.21	4.36	5.00	3.93
LP2 ↑	0.88	1.94	1.92	1.45	2.53	3.33	4.23	4.73	4.14
LP2 ↓	0.00	0.93	1.11	0.00	0.22	4.48	11.19	13.65	4.74
π* ↑	0.00	1.72	2.07	0.00	0.76	4.58	11.46	13.58	5.49
total	2.06	7.57	8.37	3.14	6.56	15.87	31.41	37.11	19.06

TABLE 8: a_N Values (in G) for All Complexes Computed at the PCM/PBE0/NO6 Level on Geometries Optimized at the PBE0/6-31G(d) Level in Solution

	TEMPO	C ₃ H ₇ I	C ₃ HF ₆ I	C ₃ F ₇ I	C ₆ H ₅ I	C ₆ F ₅ I	C ₆ H ₅ OH	C ₃ H ₇ OH	C ₃ HF ₆ OH	C ₃ F ₇ OH
gas-phase	12.74	12.79	13.07	13.10	12.85	13.01	13.44	13.18	13.67	13.64
EPR-II ^a										
gas phase	14.92	14.87	15.13	15.16	14.96	15.11	15.46	15.24	15.66	15.63
CHCl ₃	15.53 ^b	15.26	15.71	15.81	15.45	15.7	15.98	15.71	16.16	15.52
ε = 4.9										
C ₂ H ₄ Cl ₂	15.7	15.35	15.79	15.91	15.55	15.81	16.06	15.79	16.22	16.23
ε = 10.36										
ethanol	15.84	15.44	15.85	15.97	15.61	15.85	16.13	15.85	16.28	16.32
ε = 24.55										
exp	15.28	15.46		16.72	15.84	16.19	15.58	ε = 18.3	16.32	
ε = 2.02		ε = 7.0			ε = 4.6		ε = 10.0	ε = 30.0		

^a EPR-II on all atoms and N06 on iodine atom. ^b a_N value in cyclohexane (ε = 2.02) is 15.23 G.

Besides, a_N is larger for the complexes with alcohols than for those with iodine derivatives.

As is well-known, nitroxides can be considered resonance hybrids of two structures (I and II, Figure 5) of which the more polar structure II is stabilized by increasing the polarity of the solvent. Concurrently, a_N is increased by the stabilization of the resonance structure II with respect to I because the spin

density at the nitrogen nucleus increases with the relative stability of II, which involves formal charge separation within the NO moiety. So, the change of a_N can be interpreted in terms of dielectric properties of the environment and of the hydrogen-bond network.²² It is noteworthy that there is a direct connection between the HB or XB strengths (see binding energies in the preceding section) and the a_N values. Thus the trends of binding

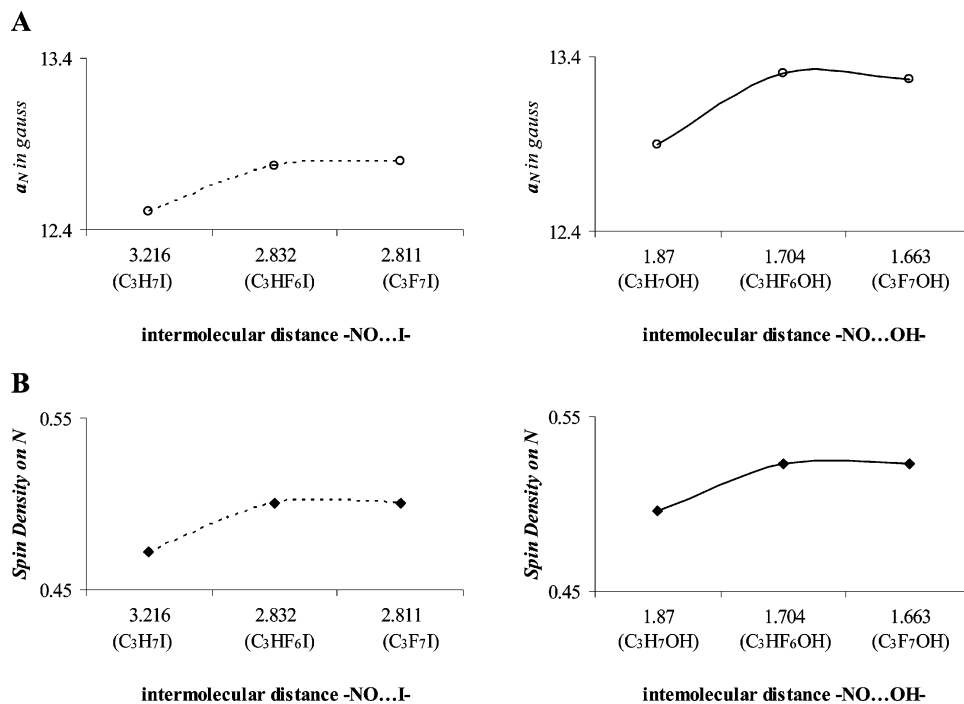


Figure 7. Correlation between intermolecular distance $\text{NO}\cdots\text{I/OH}$ (Å) and a_N (A) nitrogen spin density (B) of the $\text{TEMPO}-\text{C}_n\text{H}_n\text{I/OH}$ complexes.

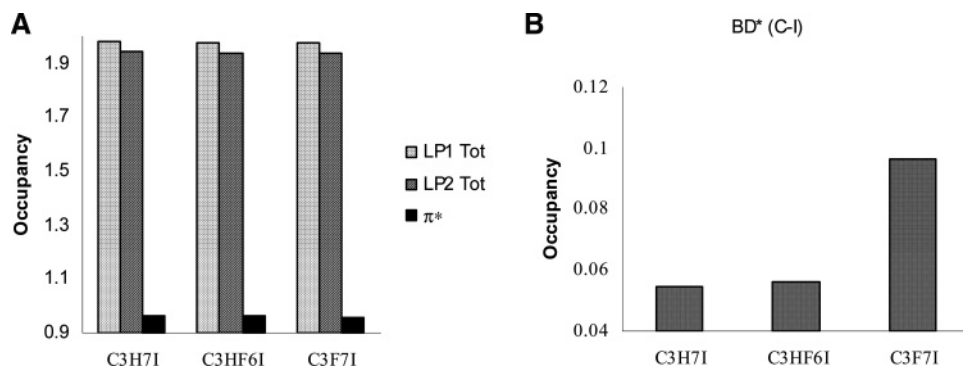


Figure 8. Occupation of oxygen lone pairs (A) and of the $(\text{BD}^*-\text{C}-\text{I/OH})^*$ antibonding orbital (B) in the complexes formed by TEMPO and iodoalkanes ($\text{C}_3\text{H}_7\text{I}$, $\text{C}_3\text{HF}_6\text{I}$, and $\text{C}_3\text{F}_7\text{I}$).

energies and of a_N values are the same: derivatives with $\text{F} >$ derivatives without F ; perfluoroalkyl $>$ perfluoroaromatic and alcohol complexes $>$ iodo complexes. At the same time, stronger HB or XB corresponds to a shorter TEMPO–hydrogen/halogen distance. Thus, stronger intermolecular interactions cause a growing of the nitrogen spin density and of its hyperfine coupling constant (see Figure 7).

In Figure 8 the fractional occupations of oxygen lone pairs and of the $(\text{C}-\text{I})^*$ antibonding orbital are plotted versus the intermolecular distances of the corresponding complexes. Comparison of the trends of distances and orbital occupations suggests that a_N is mostly affected by the $\text{LP} \rightarrow (\text{C}-\text{I/OH})^*$ charge transfer. The occupation of oxygen lone pairs (Table 9) decreases monotonically when the intermolecular distance decreases, whereas the occupation $(\text{C}-\text{I/OH})^*$ orbitals increases, i.e., the change in the LP occupation closely corresponds to the electronic charge that is transferred from the donor (TEMPO) to the acceptor.

The spin density localized on nitrogen and oxygen leads to a distinct \mathbf{g} tensor anisotropy in all nitroxides. This is related on the one hand to the relatively large spin–orbit coupling constants of heteroatoms, resulting in significant spin–orbit mixing, and on the other hand to the presence of nonbonding orbitals energetically close to the single occupied molecular

TABLE 9: Parameters for All Complexes Computed at the PBE0/NO6//PBE0/6-31G(d) Level: NBO Occupation Number of the Oxygen Lone Pairs and $(\text{C}-\text{I/OH})^*$ Antibonds and Their Respective Energies

	$\text{C}_3\text{H}_7\text{I}$	$\text{C}_3\text{HF}_6\text{I}$	$\text{C}_3\text{F}_7\text{I}$
Occupancy			
LP1 \uparrow	0.99011	0.98948	0.98953
LP1 \downarrow	0.98921	0.9845	0.98415
LP1 tot	1.97932	1.97398	1.97368
LP2 \uparrow	0.98737	0.97749	0.97665
LP2 \downarrow	0.95854	0.95883	0.95875
LP2 tot	1.94591	1.93632	1.9354
π^*	0.96234	0.96043	0.95984
Energy (au)			
LP1 \uparrow	−0.81492	−0.68592	−0.6874
LP1 \downarrow	−0.77481	−0.77949	−0.77923
LP2 \uparrow	−0.32231	−0.45355	−0.44884
LP2 \downarrow	−0.26187	−0.29967	−0.30533
$\pi^* \uparrow$	−0.27669	−0.33157	−0.34242
Occupancy			
$(\text{BD}^*\text{C}-\text{I/OH}) \uparrow$	0.02788	0.03286	0.05319
$(\text{BD}^*\text{C}-\text{I/OH}) \downarrow$	0.02687	0.02332	0.04313
$(\text{BD}^*\text{C}-\text{I/OH}) \text{ tot}$	0.05475	0.05618	0.09632
Energy (au)			
$(\text{BD}^*\text{C}-\text{I/OH}) \uparrow$	0.0818	0.06841	0.05234
$(\text{BD}^*\text{C}-\text{I/OH}) \downarrow$	0.08201	0.06968	0.05339

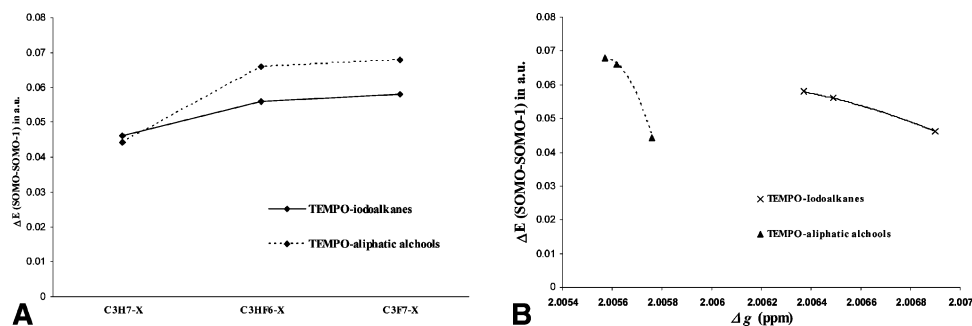


Figure 9. (A) (SOMO–SOMO-1) energy differences for the different TEMPO– C_nH_yX ($X = I$ or OH) complexes; (B) correlation between (SOMO–SOMO-1) energy differences and g tensor shifts.

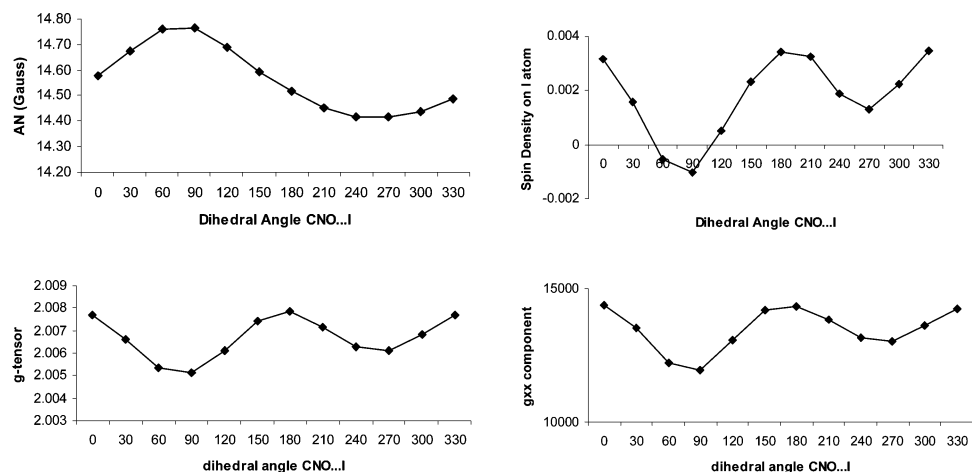


Figure 10. Correlation between CNO...I dihedral angle (deg) and A_N (A), spin density on I atom (B), g_{iso} (C), and g_{xx} (D) of the TEMPO– C_6H_5I complex.

TABLE 10: Isotropic g Tensor Shifts (in ppm) for All Complexes Computed at the PCM/PBE0/N06 Level on Geometries Optimized at the PBE0/6-31G(d) Level in Solution

	TEMPO	C_3H_7I	C_3HF_6I	C_3F_7I	C_6H_5I	C_6F_5I	C_6H_5OH	C_3H_7OH	C_3HF_6OH	C_3F_7OH
gas-phase	2.00619	2.00709	2.00673	2.00663	2.00525	2.00568	2.00580	2.00588	2.00572	2.00568
EPR-II ^a										
gas-phase	2.00624	2.00713	2.00654	2.00643	2.00527	2.00572	2.00592	2.00601	2.00585	2.00581
EPR-III ^a										
gas phase	2.00610	2.00690	2.00649	2.00637	2.00502	2.00555	2.00568	2.00576	2.00562	2.00557
CHCl ₃	2.00599	2.00680	2.00633	2.00624	2.00489	2.00540	2.00562	2.00569	2.00556	2.00555
$\epsilon = 4.9$										
$C_2H_4Cl_2$	2.00596	2.00677	2.00628	2.00621	2.00485	2.00536	2.00561	2.00569	2.00556	2.00555
$\epsilon = 10.36$										
ethanol	2.00593	2.00674	2.00625	2.00618	2.00482	2.00532	2.00560	2.00568	2.00555	2.00555
$\epsilon = 24.55$										
exp		2.00618		2.00630	2.00619	2.00645	–	–	2.00605	
		$\epsilon = 7.0$			$\epsilon = 4.6$		$\epsilon = 10.0$	$\epsilon = 18.3$	$\epsilon = 30.0$	

^a EPR-II/III on all atoms and N06 on iodine atom.

orbital (SOMO). Thus, three g shifts of significantly different magnitude are expected, with $\Delta g_{xx} > \Delta g_{yy} > \Delta g_{zz}$, the last value being always close to zero, i.e., $g_{zz} \approx g_e$. The large Δg_{xx} , directed along the NO bond (Figure 1), is particularly sensitive to the polarity of the surroundings. The most important contribution to this term comes from an electronic excitation from the SOMO-1 (an in-plane lone pair, hereafter referred to as n) to the SOMO (an out-of-plane π^* orbital), both of which are sketched in Figure 4. Furthermore, Δg_{yy} is less sensitive to the surroundings, and Δg_{zz} is basically unaffected. The dependence of the g tensor on solvent polarity is related to the selective stabilization of lone pair orbitals by polar solvents: this increases the $n \rightarrow \pi^*$ gap (Figure 9), with the consequent reduction of g tensor shifts (especially Δg_{xx}). Together with this purely electrostatic interaction, formation of solute–solvent H-bonds also concurs to the stabilization of lone pair orbitals and, once

again, to a decrease of the g tensor shifts. On the other hand, lengthening of the NO bond has a negligible effect on lone-pair orbitals, but stabilizes the π^* -SOMO: this results in a smaller $n \rightarrow \pi^*$ gap and therefore in larger g tensor values.

Interestingly, the experimental g values of the TEMPO complexes with iodine derivatives are larger than those of the corresponding alcohol species (see Table 10) and our computations show the same trend. This behavior can be related to the change in the distribution of the spin-density between three atoms: nitrogen, oxygen, and iodine. The electronic g tensor is dominated by contributions from the amount of unpaired electron on a given atom and from spin–orbit coupling. Since the spin–orbit coupling constant for the iodine atom (4303 cm^{-1}) is much larger than for nitrogen (73.3 cm^{-1}) and oxygen (151 cm^{-1}), also a quite small unpaired spin density on the halogen atom increases the g tensor value. Our computational

approach allows evaluation of the spin densities on different atoms in the complexes and in the free radical. In particular, Figure 10 compares the spin density on iodine atom and the calculated \mathbf{g} values for different intermolecular orientations. As expected from the above discussion, both g_{iso} and the g_{xx} component increase with the growing value of spin density transfer from the electron-donor to the electron-acceptor part of the complex. While the quantitative accuracy of the computational protocol employed in the evaluation of \mathbf{g} tensors (neglect of relativistic corrections and use of one-electron effective operator) could be questionable in the presence of heavy atoms,³⁷ the quite small involvement of iodine in the magnetic orbitals allows us to be fully confident about the computed general trends, which are the main goals of our study.

5. Conclusion

The present paper is devoted to a comparison between hydrogen- and halogen-bond effects on the structural and magnetic properties of nitroxide radicals. The DFT results illustrate nicely how the progressive substitution of H with F leads to shorter NO \cdots I/OH distances and increasing interaction energies (Table 6). This confirms that halogen bonds involving perfluorinated alkyl/benzyl halides and suitable donors can have strengths comparable to conventional hydrogen bonds (typical H-bonded interaction energies vary between 2 and 15 kcal/mol). While it comes out without surprise that stronger hydrogen bonds correspond to shorter intermolecular distances, our computations allow us to point out that the shortening of this distance is related to charge transfer from the $-\text{NO}$ moiety toward the I/OH antibonding orbital. From another point of view, the analysis of our data highlights the importance of the relative acceptor/donor orientation on the spectroscopic parameters, in particular on the \mathbf{g} tensors. The results reported by Figure 7 show that the position of the acceptor, especially the CNO \cdots I/OH dihedral angle, has a remarkable effect on the spin density, and consequently on the \mathbf{g} tensors.

From a more general perspective, the results of our study confirm the reliability of modern DFT-PCM approaches and the complementary role of theory and experiment in the development and validation of magnetostructural relationships.

References and Notes

- (1) Kocherginsky, N.; Swartz, H. M. *Nitroxide Spin Labels*; CRC Press: Boca Raton, FL, 1995.
- (2) Buchaklian, A. H.; Klug, C. S. *Biochemistry* **2005**, *44*, 5503.
- (3) Tedeschi, A. M.; D'Errico, G.; Busi, E.; Basosi, R.; Barone, V. *Phys. Chem. Chem. Phys.* **2002**, *4*, 2180.
- (4) Hawke, C. J.; Bosman, A. W.; Harth, E. *Chem. Rev.* **2001**, *101*, 3661.
- (5) Fisher, H. *Chem. Rev.* **2001**, *101*, 3581.
- (6) Metrangolo, P.; Neukirch, H.; Pilati, T.; Resnati, G. *Acc. Chem. Res.* **2005**, *38*, 386.
- (7) Auffinger, P.; Hays, F. A.; Westhof, E.; Shing Ho, P. *Proc. Natl. Acad. Sci. U.S.A.* **2004**, *101*, 16789.
- (8) (a) Metrangolo, P.; Resnati, G. *Chem. Eur. J.* **2001**, *7*, 2511. (b) Corradi, E.; Mille, S. V.; Messina, M. T.; Metrangolo, P.; Resnati, G. *Angew. Chem., Int. Ed.* **2000**, *39*, 1782. (c) Chu, Q. L.; Wang, Z. M.; Huang, Q. C.; Yan, C. H.; Zhu, S. Z. *J. Am. Chem. Soc.* **2001**, *123*, 11069.
- (9) (a) Nguyen, H. L.; Horton, P. N.; Hursthouse, M. B.; Legon, A. C.; Bruce, D. W. *J. Am. Chem. Soc.* **2004**, *126*, 16. (b) Crihfield, A.; Hartwell, J.; Phelps, D.; Walsh, R. B.; Harris, J. L.; Payne, J. F.; Pennington, W. T.; Hanks, T. W. *Cryst. Growth Des.* **2003**, *3*, 313. (c) Walsh, R. B.; Padgett, C. W.; Metrangolo, P.; Resnati, G.; Hanks, T. W.; Pennington, W. T. *Cryst. Growth Des.* **2001**, *1*, 165. (d) Moorthy, J. N.; Venkatakrishnan, P.; Mal, P.; Dixit, S.; Venugopalan, P. *Cryst. Growth Des.* **2003**, *3*, 581.
- (10) Mugnaini, V.; Punta, C.; Liantonio, R.; Metrangolo, P.; Recupero, F.; Resnati, G.; Pedulli, G.; Lucarini, M. *Tetrahedron Lett.* **2006**, *47*, 3265.
- (11) Improta, R.; Barone, V. *Chem. Rev.* **2004**, *104*, 1231.
- (12) (a) Barone, V.; Adamo, C.; Russo, N. *Chem. Phys. Lett.* **1993**, *212*, 5. (b) Barone, V. *J. Chem. Phys.* **1994**, *101*, 6834. (c) Barone, V. *J. Chem. Phys.* **1994**, *101*, 10666. (d) Barone, V. *Theor. Chem. Acc.* **1995**, *91*, 113. (e) Barone, V. In *Advances in Density Functional Theory*, Ed. D. P. Chong, World Sci. Publ. Co.: Singapore, 1995; Part I, p 287.
- (13) (a) Mattar, S. M. *Chem. Phys. Lett.* **1998**, *287*, 608. (b) Mattar, S. M.; Stephens, A. D. *Chem. Phys. Lett.* **2000**, *319*, 601. (c) Arbuzyanov, A. V.; Kaupp, M.; Malkin, V. G.; Reviakine, R.; Malkina, O. L. *Phys. Chem. Chem. Phys.* **2002**, *4*, 5467. (d) Mattar, S. M. *J. Phys. Chem. B* **2004**, *108*, 9449. (e) Sinnecker, S.; Reijerse, E.; Neese, F.; Lubitz, W. *J. Am. Chem. Soc.* **2004**, *126*, 3280. (f) Neugebauer, J.; Louwarse, M. J.; Belanzoni, P.; Wesolowski, T. A.; Baerends, E. J. *J. Chem. Phys.* **2005**, *109*, 445. (g) Schoneborn, J. C.; Neese, F.; Thiel, W. *J. Am. Chem. Soc.* **2005**, *127*, 5840. (h) Astashkin, A. V.; Neese, F.; Raitsimiring, A. M.; Cooney, J. J. A.; Bultman, E.; Enemark, J. H.; Neese, F. *J. Am. Chem. Soc.* **2005**, *127*, 16713. (i) Mattar, S. M. *J. Phys. Chem. A* **2007**, *111*, 251.
- (14) (a) Feller, D.; Davidson, E. R. *J. Chem. Phys.* **1988**, *88*, 5770. (b) Engels, B.; Eriksson, L. A.; Lunell, S. In *Advances in Quantum Chemistry*; Academic Press: San Diego, CA, 1996; Vol. 27, p 297. (c) Perera, S. A.; Salemi, L. M.; Bartlett, R. J. *J. Chem. Phys.* **1997**, *106*, 4061. (d) Al, Derzi, A. R.; Fan, S.; Bartlett, R. J. *J. Phys. Chem. A* **2003**, *107*, 6656.
- (15) (a) Neese, F. *J. Chem. Phys.* **2001**, *115*, 11080. (b) Ciofini, I.; Adamo, C.; Barone, V. *J. Chem. Phys.* **2004**, *121*, 6710. (c) Cheesman, J. R.; Trucks, G. W.; Keith, T. A.; Frisch, M. J. *J. Chem. Phys.* **1998**, *104*, 5497. (d) Koseki, S.; Schmidt, M. W.; Gordon, M. S. *J. Phys. Chem.* **1992**, *96*, 10768.
- (16) (a) Miertus, S.; Scrocco, E.; Tomasi, J. *Chem. Phys.* **1981**, *55*, 117. (b) Tomasi, J.; Mennucci, B.; Cammi, R. *Chem. Rev.* **2005**, *105*, 2999.
- (17) Cossi, M.; Scalmani, G.; Rega, N.; Barone, V. *J. Chem. Phys.* **2002**, *117*, 43.
- (18) Koch, A.; Thomas, S.; Kleinpeter, E. *Theochem* **1997**, *401*, 1.
- (19) (a) Rega, N.; Cossi, M.; Barone, V. *J. Am. Chem. Soc.* **1997**, *119*, 12962. (b) Rega, N.; Cossi, M.; Barone, V. *J. Am. Chem. Soc.* **1998**, *120*, 5723. (c) Improta, R.; Scalmani, G.; Barone, V. *Chem. Phys. Lett.* **2001**, *336*, 349. (d) Saracino, G. A. A.; Tedeschi, A. M.; D'Errico, G.; Improta, R.; Barone, V. *J. Phys. Chem. A* **2002**, *106*, 10700.
- (20) Cimino, P.; Pavone, M.; Barone, V. *Chem. Phys. Lett.* **2006**, *419*, 106.
- (21) Scalmani, G.; Barone, V.; Kudin, K. N.; Pomelli, C. S.; Scuseria, G. E.; Frisch, M. J. *Theor. Chem. Acc.* **2004**, *111*, 90.
- (22) (a) Rinkevicius, Z.; Telyatnyk, L.; Vahtras, O.; Ruud, K. *J. Chem. Phys.* **2004**, *121*, 5051. (b) Sinnecker, S.; Rajendran, A.; Klamt, A.; Diedendhofen, M.; Neese, F. *J. Phys. Chem. A* **2006**, *110*, 2235. (c) Barone, V.; Polimeno, A. *Phys. Chem. Chem. Phys.* **2006**, *8*, 4609. (d) Barone, V.; Brustolon, M.; Cimino, P.; Polimeno, A.; Zerbetto, M.; Zoleo, A. *J. Am. Chem. Soc.* **2006**, *128*, 15865. (e) Kaprzac, S.; Reviakine, R.; Kaupp, M. *J. Phys. Chem. B* **2007**, *111*, 811. (f) Kaprzac, S.; Reviakine, R.; Kaupp, M. *J. Phys. Chem. B* **2007**, *111*, 820.
- (23) Frisch, M. J.; et al. *Gaussian 03*, Revision D.02; Gaussian, Inc.: Pittsburgh, PA, 2003.
- (24) Adamo, C.; Barone, V. *J. Chem. Phys.* **1999**, *110*, 6158.
- (25) See: Foresman J. B.; Frisch, A. E. *Exploring Chemistry with Electronic Structure Methods* 2nd ed.; Gaussian Inc.: Pittsburgh, PA, 1996.
- (26) Adamo, C.; Barone, V.; Fortunelli, A. *J. Chem. Phys.* **1995**, *102*, 384.
- (27) Barone, V. Manuscript in preparation.
- (28) Barone, V.; Cossi, M.; Tomasi, J. *J. Chem. Phys.* **1997**, *107*, 3210.
- (29) Boys, S. F.; Bernardi, F. *Mol. Phys.* **1970**, *19*, 553.
- (30) (a) Foster, J. P.; Weinhold, F. *J. Am. Chem. Soc.* **1980**, *102*, 7211. (b) Carpenter, J. E.; Weinhold, F. *J. Mol. Struct. (Theochem)* **1988**, *169*, 41. (c) Reed, A. E.; Curtiss, L. A.; Weinhold, F. *Chem. Rev.* **1988**, *88*, 899. (d) Weinhold, F.; Landis, C. R. *Valency and Bonding: A Natural Bond Orbital Donor-Acceptor Perspective*; Cambridge University Press: Cambridge, 2005.
- (31) (a) Romaniello, P.; Lelj, F. *J. Phys. Chem. A* **2002**, *106*, 9114. (b) Valerio, G.; Raos, G.; Meille, S. V.; Metrangolo, P.; Resnati, G. *Tetrahedron Lett.* **1999**, *40*, 7519.
- (32) Boubekour, K.; Syssa-Magalé, J. L.; Palvadeau, P.; Schollhorn, B. *Tetrahedron Lett.* **2006**, *47*, 1249.
- (33) (a) Pavone, M.; Sillanpaae, A.; Cimino, P.; Crescenzi, O.; Barone, V. *J. Phys. Chem. B* **2006**, *110*, 16189. (b) Pavone, M.; Cimino, P.; De Angelis, F.; Barone, V. *J. Am. Chem. Soc.* **2006**, *128*, 4338. (c) Brancato, G.; Rega, N.; Barone, V. *J. Chem. Phys.* **2006**, *125*, 164515.
- (34) Barone, V.; Grand, A.; Minichino, C.; Subra, R. *J. Phys. Chem.* **1993**, *97*, 6355.
- (35) Carmichael, I. *J. Phys. Chem. A* **1997**, *101*, 4633.
- (36) Chipman, D. M. *Theor. Chim. Acta* **1989**, *76*, 73.
- (37) Bolvin, H. *Chem. Phys. Chem.* **2006**, *7*, 1575.